Hindawi
Advances in Civil Engineering
Volume 2019, Article ID 2618543, 15 pages
https://doi.org/10.1155/2019/2618543

Research Article

Mechanism of Dynamic Failure in Roadways with Thick and Competent Roof Strata: A Case Study

Jinshuai Guo,[1] Liqiang Ma,[2,3] Feng Ju,[1] Chengguo Zhang,[4] Fangtian Wang,[3] and Shuai Guo[1]

[1]*State Key Laboratory for Geomechanics & Deep Underground Engineering, School of Mechanics and Civil Engineering, China University of Mining and Technology, Xuzhou 221116, China*
[2]*College of Energy Engineering, Xi'an University of Science and Technology, Xi'an 710054, China*
[3]*State Key Laboratory of Coal Resources and Safe Mining, School of Mines, China University of Mining and Technology, Xuzhou 221116, China*
[4]*School of Minerals and Energy Resources Engineering, The University of New South Wales, Sydney 2052, Australia*

Correspondence should be addressed to Liqiang Ma; ckma@cumt.edu.cn

Received 1 April 2019; Accepted 4 July 2019; Published 28 July 2019

Academic Editor: Timo Saksala

Rock and coal dynamic failures have a higher chance to occur when thick and competent roof strata are presented, which can build up a high level of energy. This paper studied the fracturing characteristics of the competent roof strata during longwall face retreat and their effects on roadways' stability to gain an improved understanding of the rock dynamic failure occurred in roadways as well as the associated ground controls. The results indicated that the main reason of dynamic failure in roadways was the structural change of lateral main roof over a chain pillar, which transformed from the cantilever beam in the period of primary mining impact (PMI) to the triangular arch in the period of secondary mining impact (SMI). Based on corresponding mechanical models developed for the lateral main roof over the chain pillar, it was calculated that the force on roadways' roof in the period of SMI was 3.7 times larger than that in the period of PMI. Then, the dynamic failure control method of increasing the chain pillar width was proposed. The stress distribution and deformation of roadways with different chain pillar widths were simulated using FLAC3D. The results indicate that as the pillar width increases, the influence of secondary mining on roadways' stability decreases, and a threshold of not less than 30 m pillar width was suggested. The outcomes of this study would provide guidance for the design of chain pillars where thick and competent roof strata are presented.

1. Introduction

The extraction of coal resources at Jurassic coalfields in northern Shaanxi, China, has gradually gone deeper, and the roof strata above coal seams have changed from thin to thick and competent strata. Thick and competent strata refer to intact strata with large thickness, high strength, and undeveloped joints, which can hang out in large area without falling after coal seam mining [1, 2]. Compared with conventional roof working face (CRWF), the initial weighting interval and periodic weighting interval of thick-competent roof working face (TCRWF) are larger, which easily induce dynamic failure during mining [3, 4].

According to the studies of dynamic failure in roadways of TCRWF under primary mining impact (PMI), it is found that the width of the excavation damage zone of surrounding rock under dynamic failure is larger than that of static pressure [5, 6]. Roof thickness, strength, and distance from the coal seam are important factors to induce dynamic failure in roadways [7, 8].

With the increasing construction scale of high-yield and high-efficiency mines, double-roadway excavation has gradually become a commonly used roadways' layout

method in mining areas [9, 10]. Inevitably, roadways will be affected by the secondary mining. According to the studies of dynamic failure in roadways of TCRWF under secondary mining impact (SMI), it is found that the deformation, stress, and damaged zone width of roadways under SMI are obviously larger than those under PMI [11, 12]. To solve the deformation problem of roadways under SMI, Wang et al. proposed the support scheme of high-strength pre-bolts, Xie proposed the support scheme of prestress slit wedge tubing yielding anchors, and He et al. proposed the support scheme of intensive cable truss and small diameter high-prestressed anchor [13–15].

However, the former studies were focused on the deformation laws of the roadways under SMI and the reinforcement support. The mechanism of dynamic failure in roadways particularly under SMI has not been fully understood. Therefore, this paper analyzed the roof fracturing characteristics and the mechanism of dynamic failure in TCRWF, based on the geological conditions in northern Shaanxi. Taking the dynamic failure events of 11215 tailentry in the Xiaojihan coal mine as the example, proposing the control method to eliminate or weaken dynamic failure of roadways.

2. Geological Conditions of the Study Area

2.1. Geological Conditions of Coal Seam. Northern Shaanxi is one of the fourteen large-scale coal bases in China, including Yushen and Yuheng mine fields. The coal seams in this area are Jurassic coalfields with coal reserves of about 140 billion tons, and their annual output accounts for about 7% of the country.

Xiaojihan coal mine is the first modern mine with a production of 10 Mt/a in Yuheng mine field. Therefore, its mining experience has important guiding significance for the follow-up mines design. Xiaojihan coal mine is currently mining #2 coal seam, which is hiatal in the eastern and southwestern parts of the mine area (Figure 1). Coal seam thickness ranges from 0.68 m to 8.64 m and depth ranges from 173.98 m to 460.36 m.

2.2. Geological Conditions of Roof Strata. Taking 11215 working face as an example, the stratigraphic column of the overburden above #2 coal seam as shown in Figure 2.

According to the statistical results, the roof strata of 11215 working face have a sandstone/mudstone alternative layer structure, and the sandstone strata dominate the strata. Moreover, sandstone layers, with a thickness above 5 m account for 58.2%, indicate that the roof strata were dominated by intact sandstones. Herein, the arkose stratum (belonging to thick and competent roof strata) with a 19.8 m thick stratum was the main roof of 11215 working face and that controlled the movement of the upper strata. Therefore, we focused on the 19.8 m thick-competent arkose stratum for investigating the mechanism of dynamic failure in 11215 tailentry.

2.3. Parameters of 11215 Working Face. 11215 working face is located in Panel 11 of the Xiaojihan coal mine, and it is adjacent to the 11213 gob. The width of the chain pillar between these two working faces was 20 m, as shown in Figure 3. The 11215 face is 4888 m long in the advance direction and 280 m wide in the inclined direction. The coal seam thickness ranges from 3.6 to 6.1 m (4.5 m on average) with an average depth of 392.5 m.

To ensure the normal continuation of mining work, the double-roadway excavation method was adopted. It refers to that 11213 headentry and 11213 auxiliary headentry would be excavated at the same time before the mining of the 11213 face. After the 11213 working face was mined, 11213 headentry was abandoned, while 11213 auxiliary headentry was retained as the tailentry of 11215 working face. Therefore, 11215 tailentry (11213 auxiliary headentry) has experienced two times disturbances of 11213 face mining (PMI) and 11215 face mining (SMI).

3. Dynamic Failure Events of 11215 Tailentry

During the mining process of 11215 working face advanced from 11213 open-off cut to the finish line (SMI), many dynamic failure events occurred, and four typical cases (affect 11215 face mining) were selected for analysis. The original dimension of 11215 tailentry was 5.5 m × 3.5 m.

3.1. "4.12" Event. On April 12, 2016, the "4.12" dynamic failure event occurred when 11215 working face advanced to the location of 264 m away from the 11213 open-off cut. The roof collapse of 11215 tailentry in the advanced section was up to 1.2 m, and the hydraulic props were bent. The end of 11215 working face was blocked, as shown in Figure 4.

3.2. "5.11" Event. The "5.11" event occurred when 11215 working face advanced to the location of 396 m away from the 11213 open-off cut on May 11, 2016. Rib spalled 1.1 m in chain pillar side and 0.9 m in panel side in the advanced section of 11215 tailentry, which stopped the production of the panel. After restart production, floor heaved 1.5 m in the advanced section of 11215 tailentry when 11215 face advanced forward by 23 m, as shown in Figure 5.

3.3. "6.4" Event. On June 4, 2016, 11215 working face advanced the location of 583 m away from the 11213 open-off cut. The roof beam in the advanced section of 11215 tailentry was broken, and the roof collapse was up to 1.3 m. Rib spalling occurred in the chain pillar side and knocked down supporting hydraulic props in the tailentry, as shown in Figure 6.

3.4. "7.21" Event. 11215 working face advanced to the location of 1124 m away from the 11213 open-off cut when July 21, 2016. Severe deformations occurred within 15 m (especially within 8 m) in the advanced section of

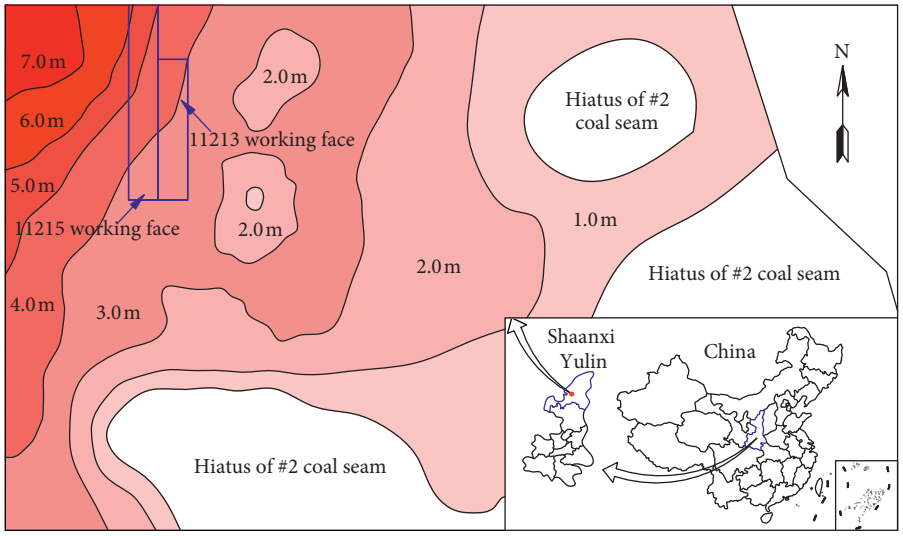

Figure 1: Thickness distribution of #2 coal seam in the Xiaojihan coal mine.

Column	Lithology	Thickness (m)	Depth (m)	Remark
	Silty mudstone	7.6	309.8	
	Arkose	10.1	319.9	
	Mudstone	10.9	331.8	
	Arkose	10.6	342.4	
	Mudstone	3.7	346.1	
	Arkose	9.9	356.0	
	Silty mudstone	5.7	361.7	
	Arkose	19.8	381.5	Main roof
	Silty mudstone	6.5	388.0	Immediate roof
	#2 coal seam	4.5	392.5	11215 working face
	Silty mudstone	4.2	396.7	
	Mudstone	2.5	399.2	
	Silty mudstone	5.0	404.2	
	Arkose	6.2	410.4	
	Silty mudstone	3.2	413.6	
	Arkose	4.6	418.2	

Figure 2: Sketch of stratigraphic columns in 11215 working face.

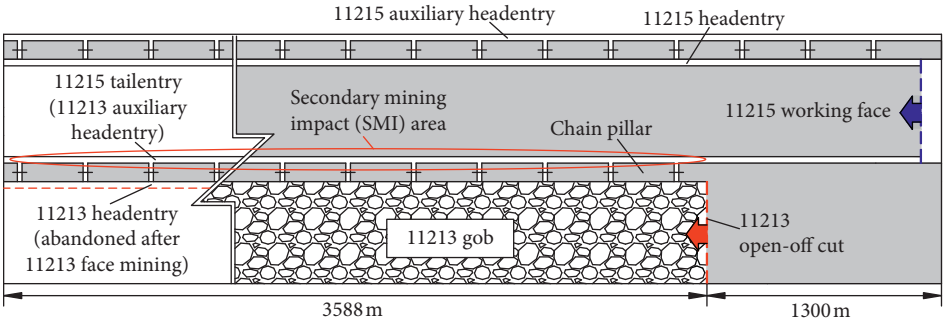

Figure 3: Layout of the working faces.

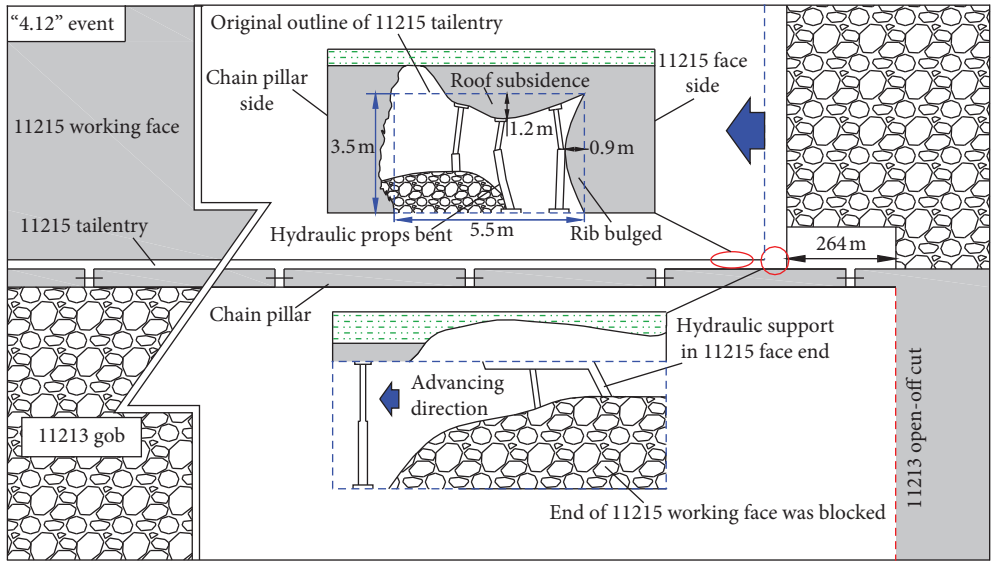

Figure 4: Sketch of the "4.12" event.

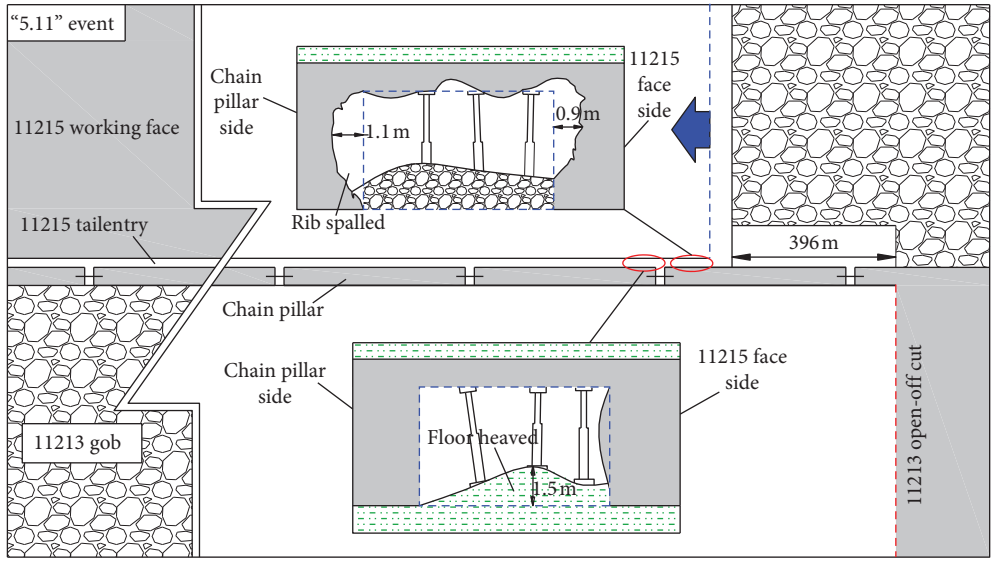

Figure 5: Sketch of the "5.11" event.

11215 tailentry. Floor heaved 0.6 m and coal wall bulged 1.2 m in the sidewall of chain pillar side, as shown in Figure 7.

4. Fracturing Characteristics of the Roof Strata in TCRWF

4.1. Fracturing Characteristics of Roof Strata. Qian et al. proposed that main roof strata would be exposed to initial fracturing and exhibited "O-X" structure, when the working face advanced forward from the open-off cut by initial weighting interval [16]. As the working face advanced further, periodic fracturing was observed in main roof strata, resulting in continuous generation of half "O-X" fracturing structure, as shown in Figure 8(a).

For the TCRWF, process and morphology of roof fracturing are similar to those of CRWF. While the fracturing affecting the range of TCRWF (i.e., the O-shaped circle) was larger than that of CRWF [17]. Therefore, the fracture line location of TCRWF is on the unmined coal side (Figure 8(b)). The probability of dynamic failure in TCRWF is greater than that of CRWF.

4.2. Relationship between Roof Fracture Line Location and Roadways' Stability. Main roof strata were tended to bending subsidence along the inclined direction of the working face, and the resulting Blocks A, B, and C were hinged to each other [16, 18]. Due to the Block B is located above the roadway, it plays an important role in the stability of the roadway and is also called key block [16, 17]. Xu et al.

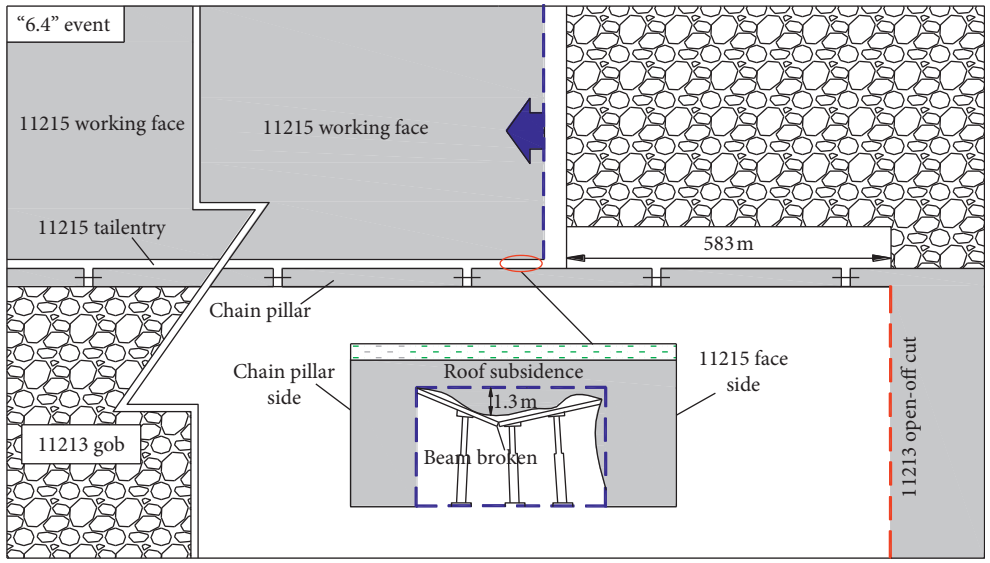

Figure 6: Sketch of the "6.4" event.

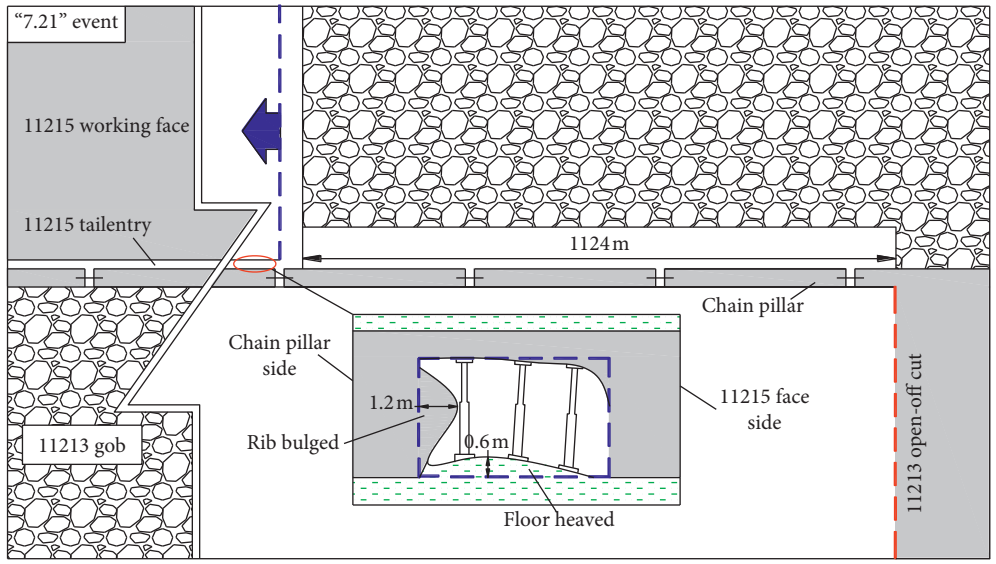

Figure 7: Sketch of the "7.21" event.

investigated the stress and deformations of the chain pillar with different fracturing structures based on the spatial locations of the chain pillar, roadway, and fracture line location of the main roof. He pointed out the relationship between deformation of roadway and fracturing structure of the main roof [19]. Wang et al. analyzed deformations of roadway under three different spatial correlations of main roof fracture line and roadway [18]. The results demonstrated that the maintenance of roadway was worst when the fracture line was located at the unmined coal side (Figure 9(a)), while the maintenance of roadway was optimal when the fracture line was located at the chain pillar side (Figure 9(c)).

5. Mechanism of Dynamic Failure in 11215 Tailentry

As mentioned above, the stability of 11215 tailentry is mainly dependent on the structure of the lateral main roof over the chain pillar. Therefore, the structures of the lateral main roof over the chain pillar under PMI (11213 working face mining) and SMI (11215 working face mining) of 11215 tailentry were established (Figure 10).

5.1. Mechanical Model of the Lateral Main Roof under PMI. In the period of PMI, Block B (key block) was not fully

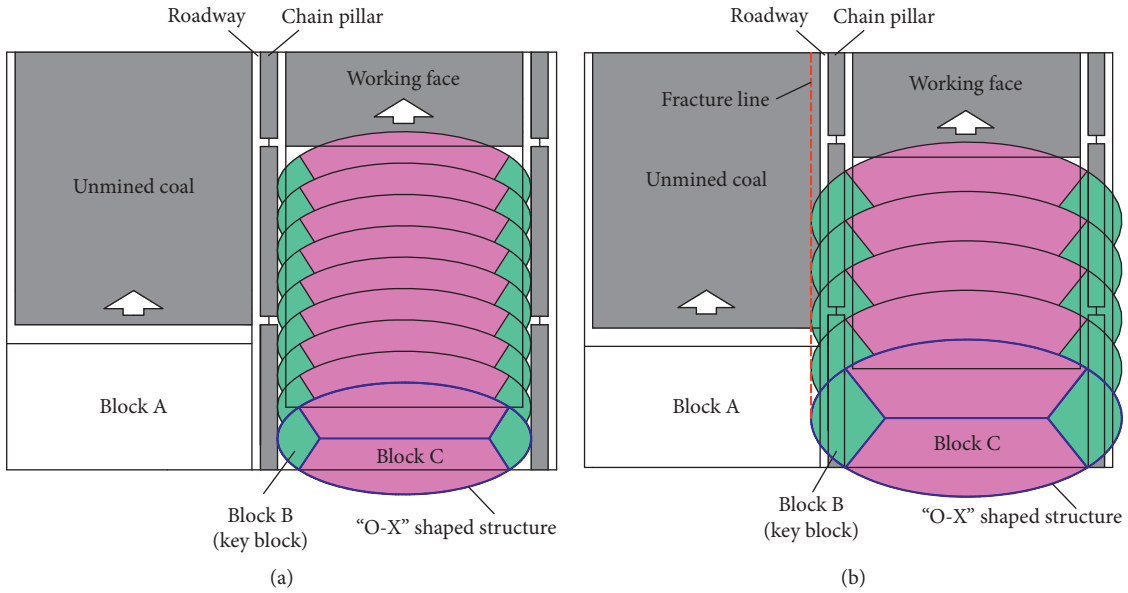

Figure 8: Fracturing structure of roof strata after mining. (a) CRWF. (b) TCRWF.

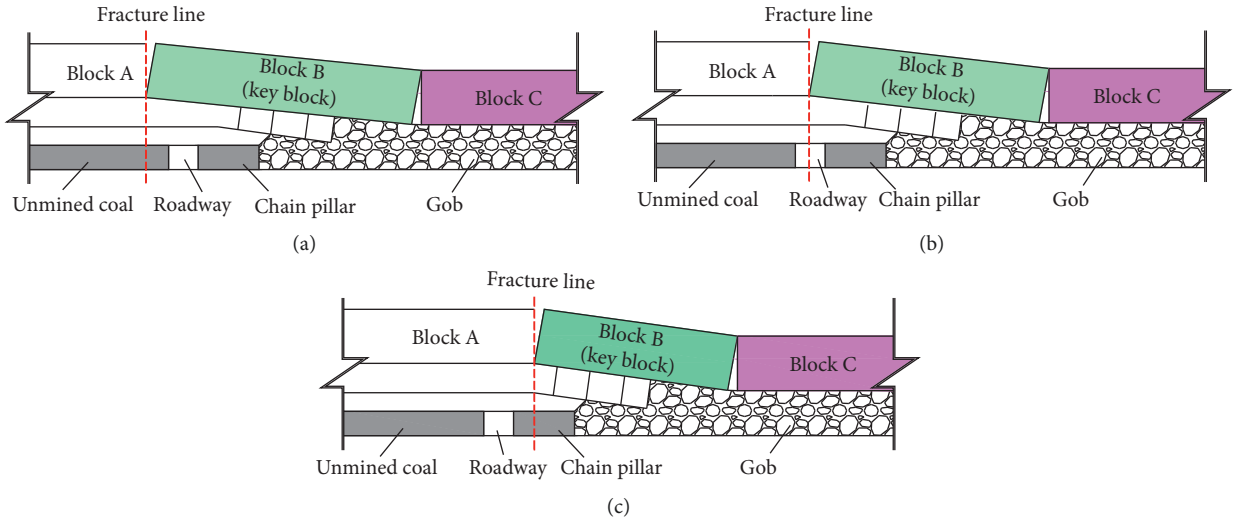

Figure 9: Structure of the lateral main roof. (a) Fracture line on the unmined coal side. (b) Fracture line above the roadway. (c) Fracture line on the chain pillar side.

detached from Block A. Hence, the mechanical model was regarded as a cantilever beam to simplify the calculation. Mechanical analysis of the cantilever beam leads to the formulae for shear force and bending moment of arbitrary cross section in the cantilever beam [20, 21], as shown in Figure 11.

5.1.1. Roof Force of 11215 Tailentry. Qian et al. proposed that the strata above and beneath (within the certain range) the main roof can be regarded as an elastic medium, which satisfies the assumptions for the Winkler elastic foundation [16, 22]. The disturbance force caused by coal seam mining on the main roof is as follows:

$$P = -ky, \tag{1}$$

where P is the disturbance force on the main roof, y is the vertical displacement of the main roof, and k is the Winkler bed coefficient.

The main roof stratum can be regarded as a semi-infinite beam, which subjected to the vertical force P and

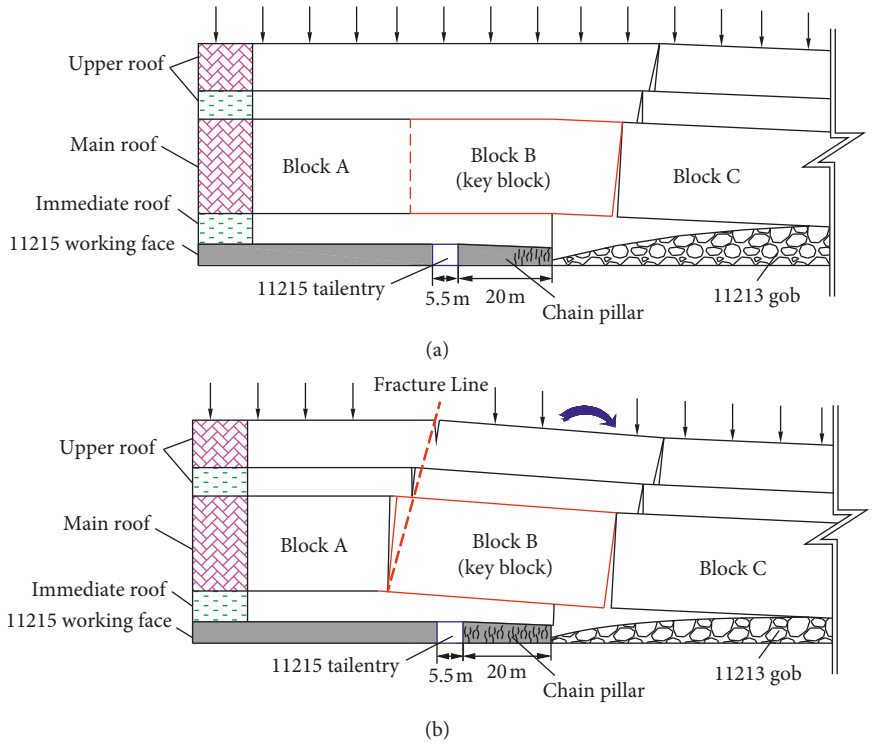

Figure 10: Structure of the lateral main roof under PMI and SMI. (a) PMI. (b) SMI.

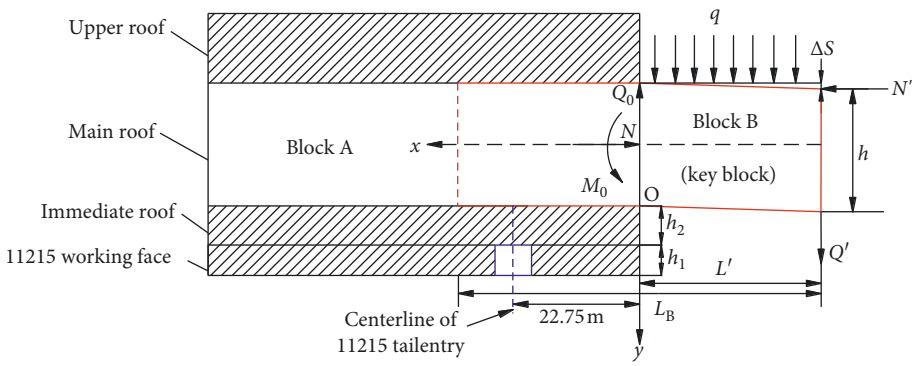

Figure 11: Mechanical model of the cantilever beam.

axial force N. According to the Timoshenko beam theory, the deflection curve equation of the main roof can be expressed as follows:

$$EIy'''' + Ny'' = P. \tag{2}$$

Herein, $E = E'/(1-v^2)$ in the plane strain state and v is the Poisson ratio.

By solving equation (2) according to boundary conditions, the deflection curve equation can be obtained as follows:

$$y = e^{-\alpha x}\left[\frac{rM_0 + 2\alpha Q_0}{EI(r-s)}\cos\beta x - \frac{2\alpha r M_0 + sQ_0}{2EI(r-s)\beta}\sin\beta x\right]. \tag{3}$$

As 11215 tailentry was beneath the cantilever beam, the roof force approximately equals the shear force on the cantilever beam. The shear force at cross section of the cantilever beam can be calculated by the following equation:

$$Q = EIy''' = e^{-\alpha x}\left[\frac{2\alpha s M_0 + rQ_0}{r-s}\cos\beta x - \frac{(2r^2 - s^2)M_0 + 2\alpha r Q_0}{2(r-s)\beta}\sin\beta x\right]. \tag{4}$$

Herein,

$$\begin{cases} M_0 = \dfrac{bh^2\left(\sigma_t + (N/bh)\right)}{6}, \\ Q_0 = qL' + Q', \\ r = \sqrt{\dfrac{k}{EI}}, \\ \alpha = \sqrt{\dfrac{r}{2} - \dfrac{S}{4}}, \\ \beta = \sqrt{\dfrac{r}{2} + \dfrac{S}{4}}, \\ S = \dfrac{N}{EI}, \end{cases} \tag{5}$$

where h is the main roof thickness (19.8 m); E is the elastic modulus of the main roof in the plane strain state (7.36 GPa); I is the section moment of the main roof ($I = bh^3/12$, where $b = 1$); Δ_S is the vertical displacement of Block B ($\Delta_S = h/6$); L_B is the length of Block B; L' is the length of the hanging part of Block B (11.7 m in this case, detected by the hydraulic drilling technique); Q' is the shear force between fractured rock blocks ($Q' = L_B(\gamma h + q)$), in which γ is the bulk density of the main roof (23 kN/m^3 in this case); q is the loads on strata above the main roof (9.25×10^3 kN/m in this case); N is the axial force ($N = L_B\ Q'/2(h - \Delta_S)$); and k is the bed coefficient of coal and immediate roof ($k = 1/\sum_{i=1}^{n}(h_i/E_i)$), in which coal seam thickness $h_1 = 4.5$ m, elastic modulus $E_1 = 1.06$ GPa, immediate roof thickness $h_2 = 6.5$ m, and elastic modulus $E_2 = 1.67$ GPa, so $k = 1.23 \times 10^3$ kN/m [23].

Substituting parameters of 11215 working face into equation (4) and defining $x = 22.75$ m (centerline of 11215 tailentry), we obtained the roof force (R_1) of 11215 tailentry under PMI was 1.0×10^5 kN.

5.1.2. Fracture Line Location of the Main Roof. The bending moment at cross section of the cantilever beam can be calculated by the following equation:

$$M = EIy'' = M_0 e^{-\alpha x}\left[\cos\beta x + \frac{\alpha(r+S) + r(Q_0/M_0)}{\beta(r-S)}\sin\beta x\right]. \tag{6}$$

The fracture line location of the main roof can be determined according to the maximum bending moment of the cantilever beam. As shown in Figure 12, the bending moment of the cantilever beam was maximized at $x = 30$ m. Therefore, the fracture line of the main roof was located 30 m inside the chain pillar.

5.2. Mechanical Model of the Lateral Main Roof under SMI. Blocks A and B were completely detached under effects of the advanced abutment stress when 11215 tailentry in the period of SMI (11215 working face advanced into the area of the 11213 gob). Meanwhile, a triangular arch structure was generated by articulation of Blocks A, B, and C [24, 25], as shown in Figure 13.

Mechanical analysis of the triangular arch structure under SMI leads to

$$\begin{aligned}
&\sum F_x = 0, \\
&T_{AB} = T_{CB}, \\
&\sum F_y = 0, \\
&Q_{AB} + \int_0^{L_1} q_1 dx + R_2 + \int_{L_1+L_h}^{D} q_2 dx + Q_{CB} = qL_B\cos\theta_1, \\
&\sum M_A = 0, \\
&\int_0^{L_1} q_1 x\,dx + R_2\left(L_1 + \frac{L_h}{2}\right) + \int_{L_1+L_h}^{D} q_2 x\,dx + Q_{CB}\left[L_B\cos\theta_1\right. \\
&\quad \left. + h\tan\theta_1 + L_C\cos(\theta_1 - \theta_2)\right] + T_{CB}\left[h_B - L_B\tan\theta_1\right. \\
&\quad \left. - L_C\tan(\theta_1 - \theta_2)\right] = \int_{h\tan\theta_1}^{h\tan\theta_1 + L_B\cos\theta_1} qx\,dx, \\
&\sum M_B = 0, \\
&\int_0^{L_1} q_1(h\tan\theta_1 + L_B\cos\theta_1 - x)dx + R_2\left(h\tan\theta_1 + L_B\cos\theta_1\right. \\
&\quad \left. - L_1 - \frac{L_h}{2}\right) + \int_{L_1+L_h}^{D} q_2(h\tan\theta_1 + L_B\cos\theta_1 - x)dx \\
&\quad + Q_{AB}(h\tan\theta_1 + L_B\cos\theta_1) = Q_{CB}L_C\cos(\theta_1 - \theta_2) \\
&\quad + T_{AB}(h - L_B\tan\theta_1) + \frac{1}{2}q(L_B\cos\theta_1)^2, \\
&\sum M_C = 0, \\
&\int_0^{L_1} q_1(h\tan\theta_1 + L_B\cos\theta_1 + L_C\cos(\theta_1 - \theta_2) - x)dx \\
&\quad + R_2\left(h\tan\theta_1 + L_B\cos\theta_1 + L_C\cos(\theta_1 - \theta_2) - L_1 - \frac{L_h}{2}\right) \\
&\quad + \int_{L_1+L_h}^{D} q_2(h\tan\theta_1 + L_B\cos\theta_1 + L_C\cos(\theta_1 - \theta_2) - x)dx \\
&\quad + Q_{AB}(h\tan\theta_1 + L_B\cos\theta_1 + L_C\cos(\theta_1 - \theta_2)) \\
&\quad = T_{AB}(h - L_B\tan\theta_1 - L_C\tan(\theta_1 - \theta_2)) \\
&\qquad + \frac{1}{2}q\left((L_B\cos\theta_1 + L_C\cos(\theta_1 - \theta_2))^2\right. \\
&\qquad \left. - (L_C\cos(\theta_1 - \theta_2))^2\right).
\end{aligned} \tag{7}$$

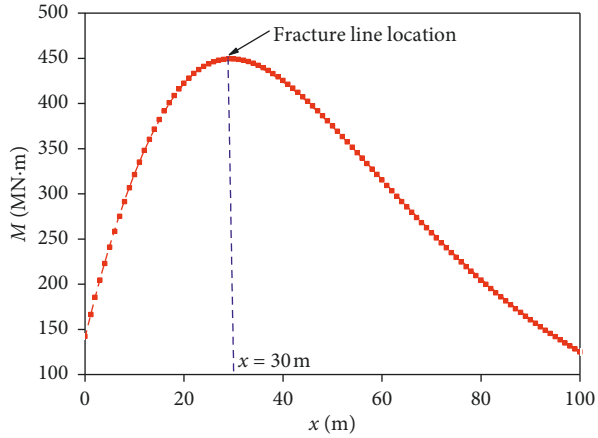

Figure 12: Distribution of bending moment in the cantilever beam.

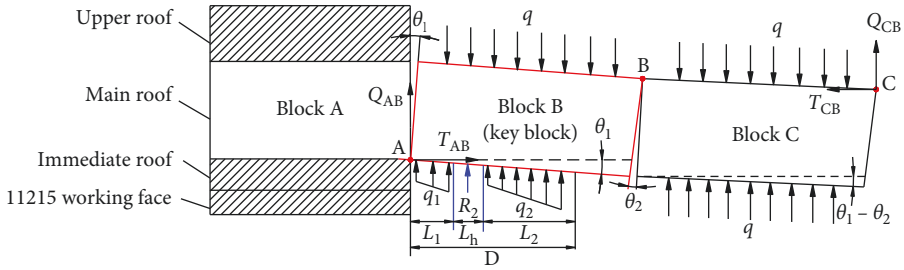

Figure 13: Mechanical model of the triangular arch structure.

The roof force (R_2) can be obtained as

$$R_2 = \frac{W_1}{W_2}. \tag{8}$$

Herein,

$$\begin{aligned} W_1 = {} & \frac{k\tan\theta_1}{3}\left[L_1^3 + D^3 - (L_1 + L_h)^3\right] \\ & + qL_B\left[L_B\cos^2\theta_1\cos(\theta_1 - \theta_2) + h\sin\theta_1\cos(\theta_1 - \theta_2)\right. \\ & \left. + L_c\cos\theta_1\cos^2(\theta_1 - \theta_2)\right] + qL_B\frac{\cos\theta_1\cos(\theta_1 - \theta_2)}{\tan(\theta_1 - \theta_2)} \\ & \cdot \left[h - L_B\tan\theta_1 - L_C\tan(\theta_1 - \theta_2)\right] \\ & - qh_BL_B\sin\theta_1 - \frac{1}{2}qL_B^2\cos^2\theta_1, \\ W_2 = {} & L_B\cos\theta_1\cos(\theta_1 - \theta_2) + h_B\tan\theta_1\cos(\theta_1 - \theta_2) \\ & + L_C\cos^2(\theta_1 - \theta_2) + \frac{\cos(\theta_1 - \theta_2)}{\tan(\theta_1 - \theta_2)}h_B \\ & - \frac{\tan\theta_1\cos(\theta_1 - \theta_2)}{\tan(\theta_1 - \theta_2)}L_B - L_C\cos(\theta_1 - \theta_2) - L_1 - \frac{L_h}{2}, \end{aligned} \tag{9}$$

where L_1 is the length of the solid coal side (4.5 m), L_2 is the width of the chain pillar (20 m), L_h is the width of 11215 tailentry (5.5 m), L_B is the length of Block B (41.7 m), L_C is the length of Block C (approximately equals to the length of Block B 41.7 m), q_1 is the supporting force by solid coal ($kx\tan\theta_1$), q_2 is the supporting force by the chain pillar ($kx\tan\theta_1$), θ_1 is the rotation angle of Block B (general was 0–10° and the average value of 5° was selected in this case), θ_2 is the rotation angle of Block C (general was 0–5° and the average value of 2.5° was selected in this case), T_{AB} is the vertical force at point A, T_{CB} is the vertical force at point C, Q_{AB} is the horizontal force at point A, and Q_{CB} is the horizontal force at point C.

Substituting parameters of 11215 working face into equation (8), we obtained the roof force (R_2) of 11215 tailentry under SMI was 3.74×10^5 kN.

Therefore, the roof force of 11215 tailentry in the period of SMI was 3.7 times larger than that in the period of PMI. The core reason for the roof force increase was the structure transformation of the lateral main roof over the chain pillar, which transformed from the cantilever beam in the period of PMI to the triangular arch in the period of SMI.

6. Controlling Methods for Dynamic Failure

The location of roof fracture line mainly depends on the roof strata thickness, lithology, and other geological conditions, as well as mining conditions such as face size, mining height, mining method, and pillar width. However, the geological conditions cannot be changed artificially,

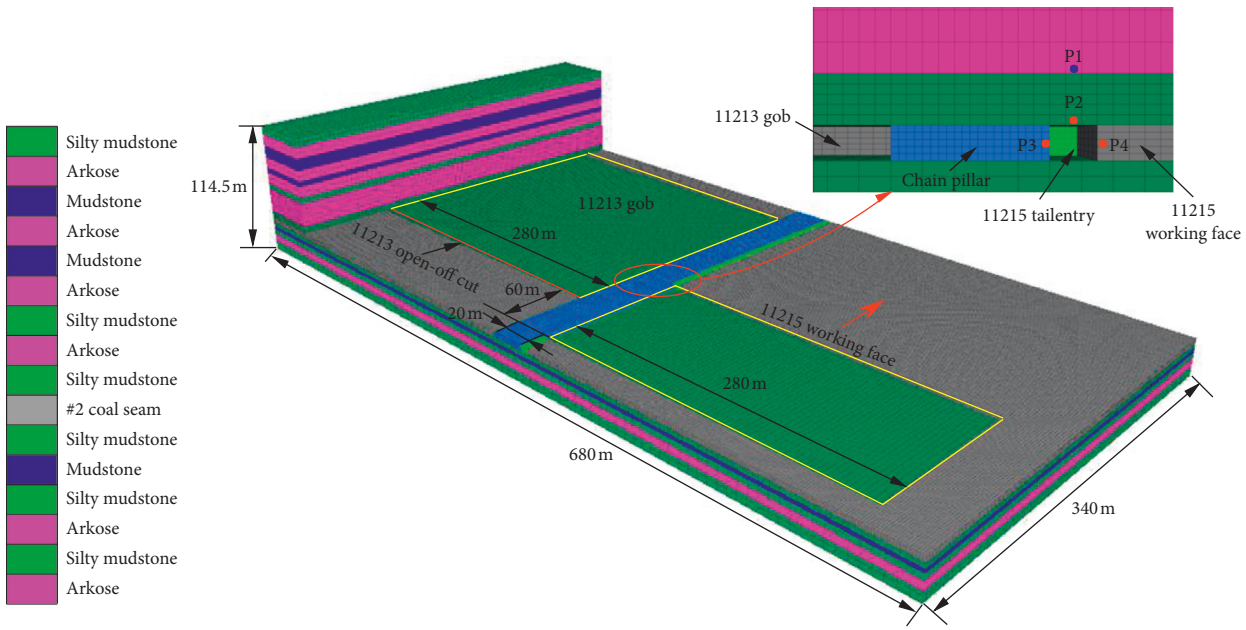

Figure 14: Model illustration.

and we can only adjust the mining parameters. Moreover, the width of the coal pillar has the most obvious impact on the location of roof fracture line. Then, we can adjust the width of the chain pillar to control the fracture line located at the chain pillar side [26, 27]. Therefore, an appropriate width of the chain pillar is of great significance to reduce the superposition of adjacent working face mining effects [28, 29].

As mentioned above, the maintenance of roadways was optimal when the fracture line was located at the chain pillar side. According to Section 4.1, the fracture line of the main roof in 11215 working face was located 30 m inside the chain pillar. Therefore, we can control the fracture line on the chain pillar side by adjusting the width of the chain pillar [30–32].

6.1. Model Setup. The effects of 11215 working face mining size (4888 × 280 m) on 11215 tailentry cannot be completely simulated by FLAC3D at full scale in great details due to computational limitations. Hence, a representative section was modelled in this study. The fundamental laws of roof stress and deformation in 11215 tailentry under PMI and SMI were simulated.

A numerical model with dimensions of 680 × 340 × 114.5 m was established to simulate the strata in the study area (Figure 14). Displacement constraints were applied to their lateral and bottom boundaries [33]. An 84.5 m thick stratum immediately above #2 coal seam was modelled, and the rest of the overburden by pressure was exerted on the top of the model. The Mohr–Coulomb failure criterion was used in the model [34].

Four monitoring points were setup in the model. More specifically, P1 was responsible for monitoring the variation of main roof stress, P2 was responsible for monitoring the variation of roof subsidence of 11215 tailentry, and P3 and P4 were responsible for monitoring the variation of width reduction of the 11215 tailentry. Table 1 summarizes relevant parameters of strata in the model.

6.2. Characteristics of 11215 Tailentry under PMI and SMI. The roof stress and deformation characteristics of 11215 tailentry with 20 m pillar width under PMI and SMI as shown in Figure 15. The roof stress of 11215 tailentry under SMI was 1.13 times that under PMI. The value was smaller than the results of theoretical calculation, which was due to the limit of the simulation size. The roof subsidence and the width reduction of 11215 tailentry under SMI were 1.41 times and 1.73 times that under PMI. Therefore, the deformation of 11215 tailentry under SMI was more serious than that under PMI.

6.3. Appropriate Width of the Chain Pillar. Roof stress and deformation of 11215 tailentry at a width of the chain pillar of 20 m, 30 m, 40 m, and 50 m were simulated. Roof stress and deformation data of 11215 tailentry were selected to analyze when 11215 working face advanced to the location of the 11213 open-off cut.

6.3.1. Roof Stress Evolution Laws. When the width of the chain pillar increased from 20 m to 30 m, the average roof stress of 11215 tailentry was reduced by 14.4% (from 1.39 times to 1.19 times the initial stress). When the width of the chain pillar increased from 30 m to 40 m, the average roof stress of 11215 tailentry was reduced by 4.2% (from 1.19 times to 1.14 times the initial stress). When the width of the chain pillar increased from 40 m to 50 m, the average roof stress of 11215 tailentry was reduced by 2.6% (from 1.14 times the initial stress to 1.11 times the initial stress), as shown in Figure 16.

Table 1: Rock mechanical parameters.

Number	Strata	Density (kg/m^3)	Bulk modulus (GPa)	Shear modulus (GPa)	Cohesion (MPa)	Friction angle (°)	Tensile strength (MPa)
1	#2 coal seam	1467	0.44	0.36	2.1	24	1.92
2	Silty mudstone	2566	1.36	0.42	5.41	32.9	1.62
3	Mudstone	2550	1.28	0.36	5.1	28	1.22
4	Arkose	2630	4.92	2.4	13.5	30.2	4.31

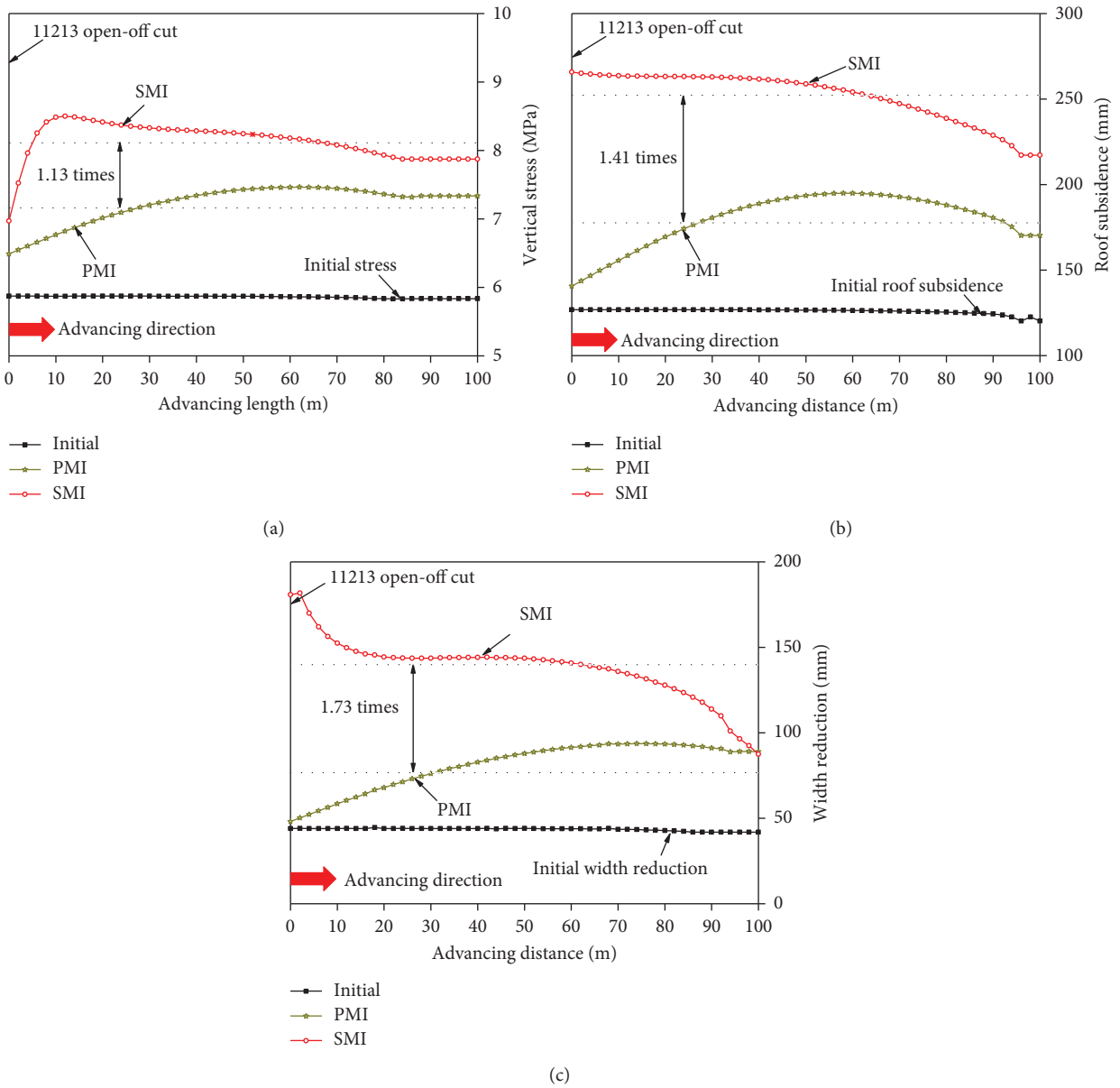

Figure 15: Characteristics of 11215 tailentry under PMI and SMI. (a) Roof stress. (b) Roof subsidence. (c) Width reduction.

6.3.2. Deformation Evolution Laws. The average roof subsidence of 11215 tailentry was reduced by 16.6%, 10.2%, and 8.1%, respectively, and average width reduction was reduced by 32.7%, 15.0%, and 11.0%, respectively, when the width of the chain pillar increased from 20 m to 30 m, 40 m, and 50 m (Figure 17).

6.3.3. Distribution of Damaged Zone. Meanwhile, distributions of the damaged zone in the chain pillar at the advanced section 20 m of 11215 tailentry were analyzed (Figure 18). The damaged zones on both sides of the chain pillar were connected when the width of the chain pillar was 20 m. When the width of the chain pillar was 30 m,

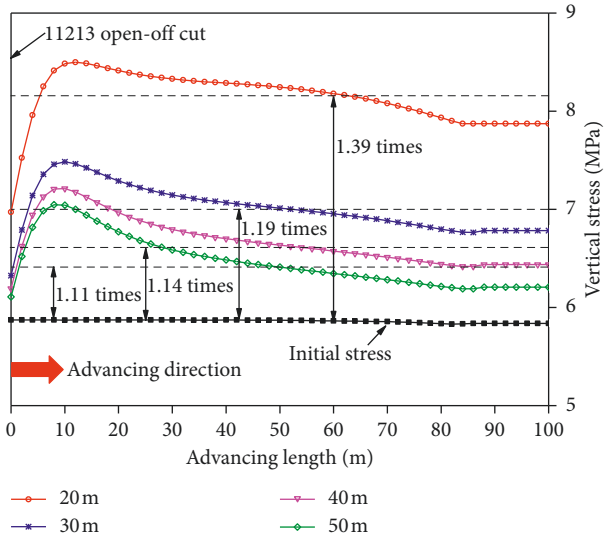

Figure 16: Variation of roof stress at different widths of the chain pillar.

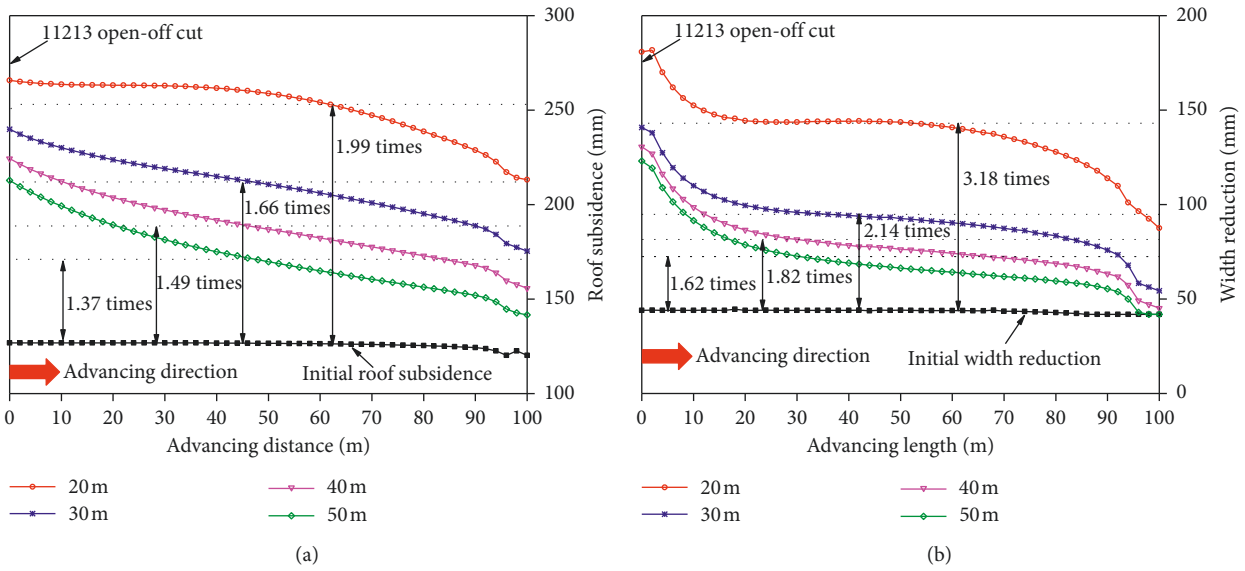

Figure 17: Deformations at different widths of the chain pillar. (a) Roof subsidence. (b) Width reduction.

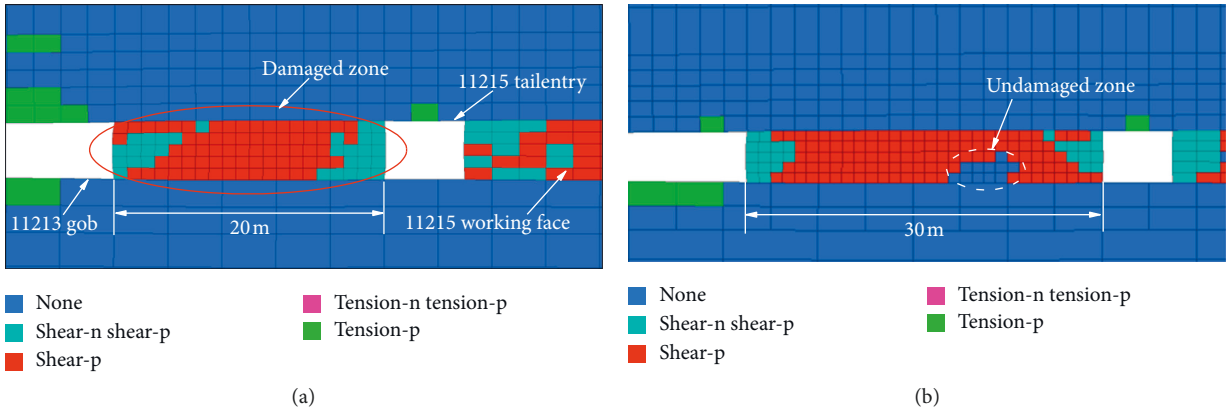

Figure 18: Continued.

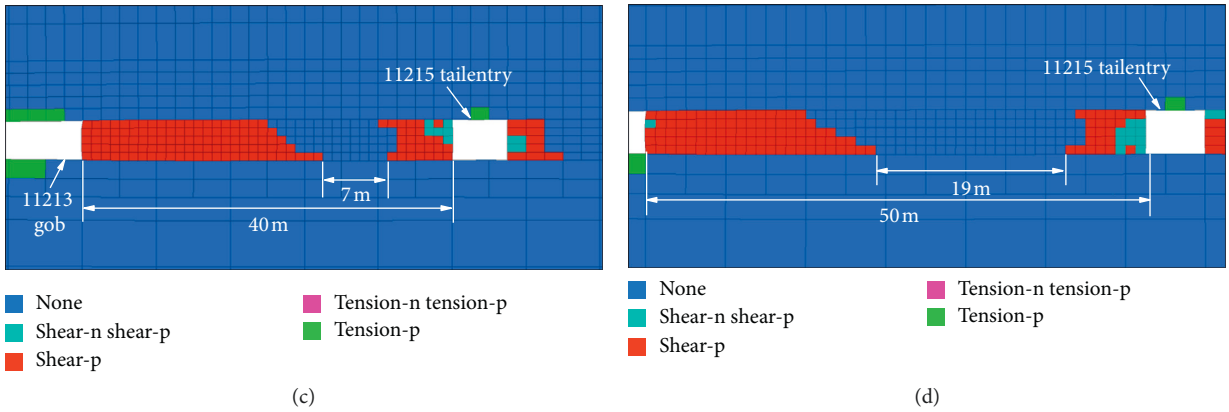

Figure 18: Distribution of the damaged zone in variable width chain pillars. (a) Width of the chain pillar was 20 m. (b) Width of the chain pillar was 30 m. (c) Width of the chain pillar was 40 m. (d) Width of the chain pillar was 50 m.

certain areas in the middle of the chain pillar were undamaged. When the width of the chain pillar was 40 m, a 7 m undamaged zone was observed in the middle of the chain pillar. When the width of the chain pillar was 50 m, a 19 m undamaged zone was observed in the middle of the chain pillar.

6.3.4. Appropriate Width of the Chain Pillar. In conclusion, the impact of 11215 working face mining (SMI) on 11215 tailentry decreased as the width of the chain pillar increased. In addition, the degree of roof stress and deformation decreased when the width of the chain pillar increased from 20 m to 30 m was significantly larger than that when the width of chain pillar increased from 30 m to 40 m and 50 m. Therefore, the simulation results of 11215 tailentry indicated that 30 m was a critical value of the pillar width. When the pillar width was less than 30 m, it cannot reduce the superposition of mining impact of 11213 and 11215 working faces.

According to the research results of the relationships between the roof fracture line location and the roadways' stability, the maintenance of roadways was optimal when the fracture line was located at the chain pillar side [35, 36]. The theoretical calculation results indicated that the fracture line of the main roof was located at 30 m. Overall, considering both numerical simulation and theoretical calculation results, the width of the coal pillar should be above 30 m to maintain the stability of 11215 tailentry.

7. Conclusions

(1) This paper studied the fracturing characteristics of the roof strata during longwall face retreat. The fracture line location of the roof structure has a significant impact on the roadways' stability. The maintenance of roadways was optimal when the fracture line was located at the chain pillar side.

(2) The mechanism of dynamic failure in roadways of TCRWF was analyzed. The main reason was the structure transformation of the lateral main roof over the chain pillar, which transformed from the cantilever beam in the period of PMI to triangular arch in the period of SMI. The roof force of roadways in the period of SMI was 3.7 times larger than that in the period of PMI.

(3) The dynamic failure control method of increasing the chain pillar width was proposed. The impact of working face mining (SMI) on roadways decreased as the width of the chain pillar increased. However, the impact degree degraded when the chain pillar width exceeded 30 m. Hence, the reasonable chain pillar width should be above 30 m.

Data Availability

The data used to support the findings of this study are included within the article.

Conflicts of Interest

The authors declare that they have no conflicts of interest.

Acknowledgments

This work was supported by the Fundamental Research Funds for the Central Universities (2018BSCXC39) and Postgraduate Research & Practice Innovation Program of Jiangsu Province (KYCX18_1979).

References

[1] J. Coggan, F. Gao, D. Stead, and D. Elmo, "Numerical modelling of the effects of weak immediate roof lithology on coal mine roadway stability," *International Journal of Coal Geology*, vol. 90-91, no. 1, pp. 100–109, 2012.

[2] Z. K. Zhang, L. G. Wang, R. L. Shan, and Y. L. Lu, "Support technology of high resistant and yielding property for deep roadway under dynamic pressure," *Journal of Mining and Safety Engineering*, vol. 29, no. 1, pp. 33–37, 2012.

[3] M. R. Islam and R. Shinjo, "Numerical simulation of stress distributions and displacements around an entry roadway with igneous intrusion and potential sources of seam gas emission of the Barapukuria coal mine, NW Bangladesh," *International Journal of Coal Geology*, vol. 78, no. 4, pp. 249–262, 2009.

[4] D. Elmo and D. Stead, "An integrated numerical modelling-discrete fracture network approach applied to the characterisation of rock mass strength of naturally fractured pillars," *Rock Mechanics and Rock Engineering*, vol. 43, no. 1, pp. 3–19, 2010.

[5] H. Wang, Y. Jiang, S. Xue et al., "Assessment of excavation damaged zone around roadways under dynamic pressure induced by an active mining process," *International Journal of Rock Mechanics and Mining Sciences*, vol. 77, pp. 265–277, 2015.

[6] J. P. Zhang, L. M. Liu, X. Yan, and Y. H. Li, "Asymmetrical support technology for dynamic pressure roadway: a case study from Guotun coal mine in China," *Geotechnical and Geological Engineering*, vol. 37, no. 2, pp. 823–832, 2019.

[7] H. E. Lawson, D. Tesarik, M. K. Larson, and H. Abraham, "Effects of overburden characteristics on dynamic failure in underground coal mining," *International Journal of Mining Science and Technology*, vol. 27, no. 1, pp. 121–129, 2017.

[8] A. T. Iannacchione and S. C. Tadolini, "Occurrence, predication, and control of coal burst events in the U.S," *International Journal of Mining Science and Technology*, vol. 26, no. 1, pp. 39–46, 2016.

[9] X. Y. Zhang, J. C. Chang, and L. Wang, "Study on surrounding rock stress and reasonable pillar of mining induced roadway groups in deep well," *Journal of Mining and Safety Engineering*, vol. 27, no. 1, pp. 72–76, 2010.

[10] J. Z. Li, J. B. Zhang, J. L. Hou, L. Wang, Z. Q. Yin, and C. M. Lim, "Multiple disturbance instability mechanism of dynamic pressure roadway and mining sequence optimization," *Journal of Mining and Safety Engineering*, vol. 32, no. 3, pp. 439–445, 2015.

[11] Y. K. Li, Z. Hao, B. Li, T. H. Huo, and H. Zhang, "Plastic zone evolution law and enhanced support technology of surrounding rock in[JP]gateway retained along goaf with double gateway layout," *Coal Science and Technology*, vol. 45, no. 6, pp. 118–123, 2017.

[12] X. Z. Hua, Y. Ming, Q. J. Liu, and P. Yang, "Model test on evolution mechanism of floor heave in gob-side retaining entry of deep mine," *Journal of Mining and Safety Engineering*, vol. 35, no. 1, pp. 1–9, 2018.

[13] Q. Z. Wang, X. L. Lin, X. W. Jing, and J. Kong, "Secondary mining roadway damage mechanism and control technology," *Metal Mine*, vol. s1, pp. 649–652, 2009.

[14] J. Xie, "Deformation mechanism and control technology of roadway with two-time kinetic pressure," *Metal Mine*, vol. 3, no. 465, pp. 80–83, 2015.

[15] F. L. He, D. P. Yin, H. Yan, Q. Li, and H. Z. Yang, "Experiment of powerful anchor truss support system applied to mining roof falling gateway," *Coal Science and Technology*, vol. 39, no. 2, pp. 1–5, 2011.

[16] M. G. Qian, X. X. Miao, and J. L. Xu, *Key Strata Theory in Ground Control*, China University of Mining and Technology Press, Xuzhou, China, 2003.

[17] J. H. Liu, F. X. Jiang, G. J. Sun, S. X. Lu, and D. F. Zhang, "Selection of advanced hydraulic support in gob-side entry of fully mechanized caving face of deep mine," *Chinese Journal of Rock Mechanics and Engineering*, vol. 31, no. 11, pp. 2232–2239, 2012.

[18] H. S. Wang, D. S. Zhang, S. G. Li, L. Wang, and L. Z. Wu, "Rational width of narrow coal pillar based on the fracture line location of key rock B in main roof," *Journal of Mining and Safety Engineering*, vol. 31, no. 1, pp. 10–16, 2014.

[19] X. L. Xu, H. Wei, S. C. Tian, and B. Zhang, "Study on influence law of coal pillar size on roof break structure and fracture development in fully mechanized working face," *Journal of the China Coal Society*, vol. 40, no. 4, pp. 850–855, 2015.

[20] Y. F. Li and X. Z. Hua, "The Stability of key block and calculating the width of roadside backfill in a secondary gob-side entry retaining," *Journal of Mining and Safety Engineering*, vol. 29, no. 6, pp. 783–789, 2012.

[21] S. Y. Chen, C. S. Song, Z. B. Guo, and Y. Wang, "Asymmetric deformation mechanical mechanism and control countermeasure for deep roadway affected by mining," *Journal of China Coal Society*, vol. 41, no. 1, pp. 246–254, 2016.

[22] Y. Pan and S. T. Gu, "Mechanical properties of hard roof based on assumptions of soften foundation and elastic foundation," *Chinese Journal of Rock Mechanics and Engineering*, vol. 34, no. 7, pp. 1402–1414, 2015.

[23] Q. Sun, J. X. Zhang, F. Ju, N. Zhou, and Q. Zhang, "Laws and mechanism of strata behaviors in backfill mining," *Journal of Mining and Safety Engineering*, vol. 34, no. 2, pp. 310–316, 2017.

[24] M. Mathey and J. N. Merwe, "Critique of the South African squat coal pillar strength formula," *Journal of the Southern African Institute of Mining and Metallurgy*, vol. 116, no. 2, pp. 291–299, 2016.

[25] X. L. Xu, S. C. Tian, J. S. Li, and X. B. Mao, "Influence law of roof breaking structure of working face on roadway pressure in Xiaojihan coal mine," *Journal of China Coal Society*, vol. 42, no. 2, pp. 308–314, 2017.

[26] X. Y. Yu, Q. Wang, B. C. Zhao, Q. S. Bao, and H. T. Wang, "Study on reasonable width of pillar between roadways in large mining height face with double roadways layout," *Chinese Journal of Rock Mechanics and Engineering*, vol. 34, pp. 3328–3336, 2015.

[27] G. C. Zhang and F. L. He, "Pillar width determination and surrounding rocks control of gob-side entry with large cross-section and fully-mechanized mining," *Rock and Soil Mechanics*, vol. 37, no. 6, pp. 1721–1728, 2016.

[28] B. A. Poulsen, "Coal pillar load calculation by pressure arch theory and near field extraction ratio," *International Journal of Rock Mechanics and Mining Sciences*, vol. 47, no. 7, pp. 1158–1165, 2010.

[29] M. Jawed and R. K. Sinha, "Design of rhombus coal pillars and support for roadway stability and mechanizing loading of face coal using SDLs in a steeply inclined thin coal seam-a technical feasibility study," *Arabian Journal of Geosciences*, vol. 11, no. 15, p. 415, 2018.

[30] J. Zhang, F. Jiang, S. Zhu, and L. Zhang, "Width design for gobs and isolated coal pillars based on overall burst-instability prevention in coal mines," *Journal of Rock Mechanics and Geotechnical Engineering*, vol. 8, no. 4, pp. 551–558, 2016.

[31] Q. Wang, H. K. Gao, B. Jiang et al., "Research on reasonable coal pillar width of roadway driven along goaf in deep mine," *Arabian Journal of Geosciences*, vol. 10, no. 21, p. 466, 2017.

[32] V. M. Seryakov, S. V. Rib, and V. N. Fryanov, "Stress state of a coal pillar in fully mechanized longwall mining in dislocation zone," *Journal of Mining Science*, vol. 53, no. 6, pp. 1001–1008, 2017.

[33] T. Sherizadeh and P. H. S. W. Kulatilake, "Assessment of roof stability in a room and pillar coal mine in the U.S. using three-dimensional distinct element method," *Tunnelling and Underground Space Technology*, vol. 59, pp. 24–37, 2016.

[34] A. Jaiswal and B. K. Shrivastva, "Numerical simulation of coal pillar strength," *International Journal of Rock Mechanics and Mining Sciences*, vol. 46, no. 4, pp. 779–788, 2009.

[35] J. Guo, L. Ma, Y. Wang, and F. Wang, "Hanging wall pressure relief mechanism of horizontal section top-coal caving face

and its application-a case study of the Urumqi coalfield, China," *Energies*, vol. 10, no. 9, p. 1371, 2017.

[36] S. Zhang, Y. Li, B. Shen, X. Sun, L. Gao, and L. Q. Gao, "Effective evaluation of pressure relief drilling for reducing rock bursts and its application in underground coal mines," *International Journal of Rock Mechanics and Mining Sciences*, vol. 114, pp. 7–16, 2019.